Journal of Power Sources 242 (2013) 768–774

Contents lists available at SciVerse ScienceDirect

Journal of Power Sources

journal homepage: www.elsevier.com/locate/jpowsour

Short communication

Synthesis and cathode properties of a cubic rocksalt-type Si-doped Li_2NiTiO_4 for lithium-ion batteries

Yusuke Kawano [a], Ayuko Kitajou [b], Shigeto Okada [c,*]

[a] Interdisciplinary Graduate School of Engineering Sciences, Kyushu University, 6-1 Kasuga-koen, Kasuga 816-8580, Japan
[b] Research and Education Center of Carbon Resources, Kyushu University, 6-1 Kasuga-koen, Kasuga 816-8580, Japan
[c] Institute for Materials Chemistry and Engineering, Kyushu University, 6-1 Kasuga-koen, Kasuga 816-8580, Japan

HIGHLIGHTS

- $Li_2NiSi_xTi_{1-x}O_4$ could be obtained by sol–gel method in the whole $0 \leq x \leq 0.2$ regions.
- The energy densities at a low rate of obtained Li_2NiTiO_4 and $Li_2NiSi_{0.1}Ti_{0.9}O_4$ were equivalent to that of $LiCoO_2$.
- The framework of obtained products was stable enough to maintain the charge-discharge processes.

ARTICLE INFO

Article history:
Received 22 January 2013
Received in revised form
21 May 2013
Accepted 24 May 2013
Available online 5 June 2013

Keywords:
Lithium-ion battery
Si-doped titanates
Cubic rocksalt
Li_2NiTiO_4

ABSTRACT

$Li_2NiSi_xTi_{1-x}O_4$ was obtained by the sol–gel method under ambient pressure in the whole $0 \leq x \leq 0.2$ regions. The lattice constant did not change, but the crystallinity decreased by increasing the Si doping level. The discharge capacities at the rate of 0.32 mA g^{-1} for the obtained Li_2NiTiO_4 and $Li_2NiSi_{0.1}Ti_{0.9}O_4$ were 153.4 mAh g^{-1} and 145.5 mAh g^{-1}, respectively. The energy densities of the Li_2NiTiO_4 (598 mWh g^{-1}) and $Li_2NiSi_{0.1}Ti_{0.9}O_4$ (567 mWh g^{-1}) obtained at the rate of 0.32 mA g^{-1} were equivalent to that of $LiCoO_2$. Moreover, the discharge capacities of Li_2NiTiO_4 and $Li_2NiSi_{0.1}Ti_{0.9}TiO_4$ remained at 57.1 mAh g^{-1} and 75.6 mAh g^{-1} even after 20 cycles, respectively. In addition, the framework of Li_2NiTiO_4 and $Li_2NiSi_xTi_{1-x}O_4$ was stable enough to maintain its charge–discharge processes at the first cycle by expansion and contraction of the lattice accompanying the extraction/insertion of lithium.

1. Introduction

In recent years, the need for a lithium ion battery with high voltage and high energy density has become more urgent because of the proliferation of advanced portable electronic devices and hybrid vehicles. Li-ion batteries constitute the current state of the art in high-energy-density rechargeable energy storage cells. Further advances in energy density have been limited by the energy density of their cathode electrodes. Commercially available Li-ion batteries generally consist of layered rocksalt type transition metal oxides like $LiCoO_2$ and$LiNiO_2$ as the cathode material, graphite carbon as the anode material and non-aqueous organic solvents containing Li salts as the electrolyte solution. Although $LiCoO_2$has an acceptable capacity of 140 mAh g^{-1} at 3.9 V, $LiNiO_2$ shows the larger capacity of 200 mAh g^{-1}. However, this compound has some problem that is poor cyclability and low thermal stability [1–3]. In contrast, $LiNi_{0.5}Mn_{0.5}O_2$ has a layered structure with a space group of *R*-3*m*, and contains divalent nickel and tetravalent manganese. Because Mn^{4+} is more stable than that of Ni^{4+}, this compound has higher thermal stability than that of $LiCoO_2$ and $LiNiO_2$, and performs extremely well as a cathode active material for rechargeable lithium batteries, providing over 30 cycles with a capacity of 200 mAh g^{-1} [4,5].

In the same way, we focused on Li_2NiTiO_4 ($LiNi_{0.5}Ti_{0.5}O_2$) as the other cathode candidate with divalent nickel and tetravalent transition metal, titanium, because Ti^{4+} is more stable and light weight than Mn^{4+} [6]. Li_2NiTiO_4 has 3 kinds of crystal structure with *R*-3*m* [7], *C*2/*c*[8] and *Fm*-3*m* space group. Among them, cubic rocksalt Li_2NiTiO_4 with *Fm*-3*m* space group showed the largest discharge capacity of about 100 mAh g^{-1}, although Li coexists with transition metals at the 4*b* octahedral site. Moreover, the reported discharge capacities of cubic rocksalt Li_2MTiO_4 (M = Co, Mn) are about 144 mAh g^{-1} (Li_2CoTiO_4) and 190 mAh g^{-1} at 60 °C (Li_2MnTiO_4), respectively [9,10]. In addition, the cubic rocksalt structure

* Corresponding author. Tel./fax: +81 92 583 7841.
E-mail addresses: s-okada@cm.kyushu-u.ac.jp, s-okada@mx3.canvas.ne.jp (S. Okada).

0378-7753/$ – see front matter © 2013 Elsevier B.V. All rights reserved.
http://dx.doi.org/10.1016/j.jpowsour.2013.05.131

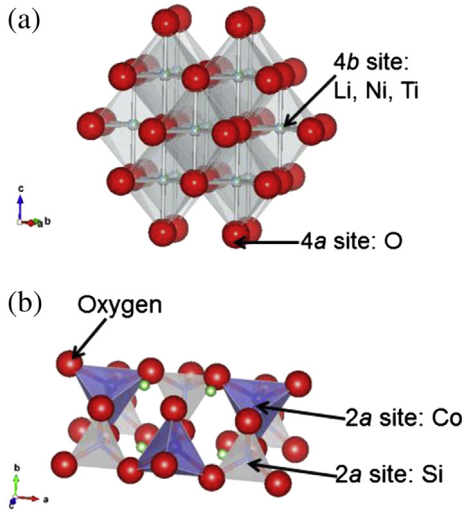

Fig. 1. Crystal structure of (a) cubic racksalt-type Li_2NiTiO_4 and (b) Li_2NiSiO_4.

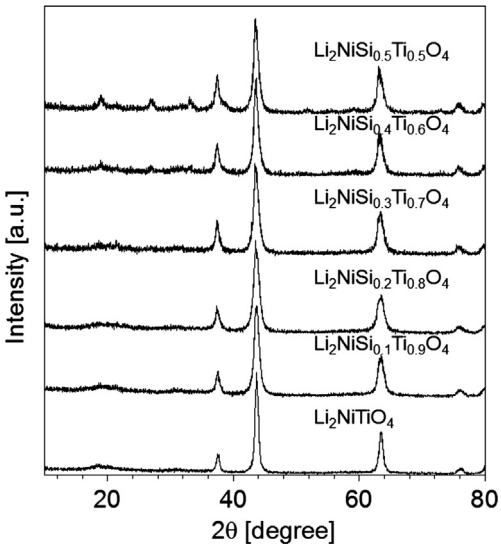

Fig. 2. X-ray diffraction patterns for the obtained $Li_2NiSi_xTi_{1-x}O_4$ ($x = 0 \sim 0.5$).

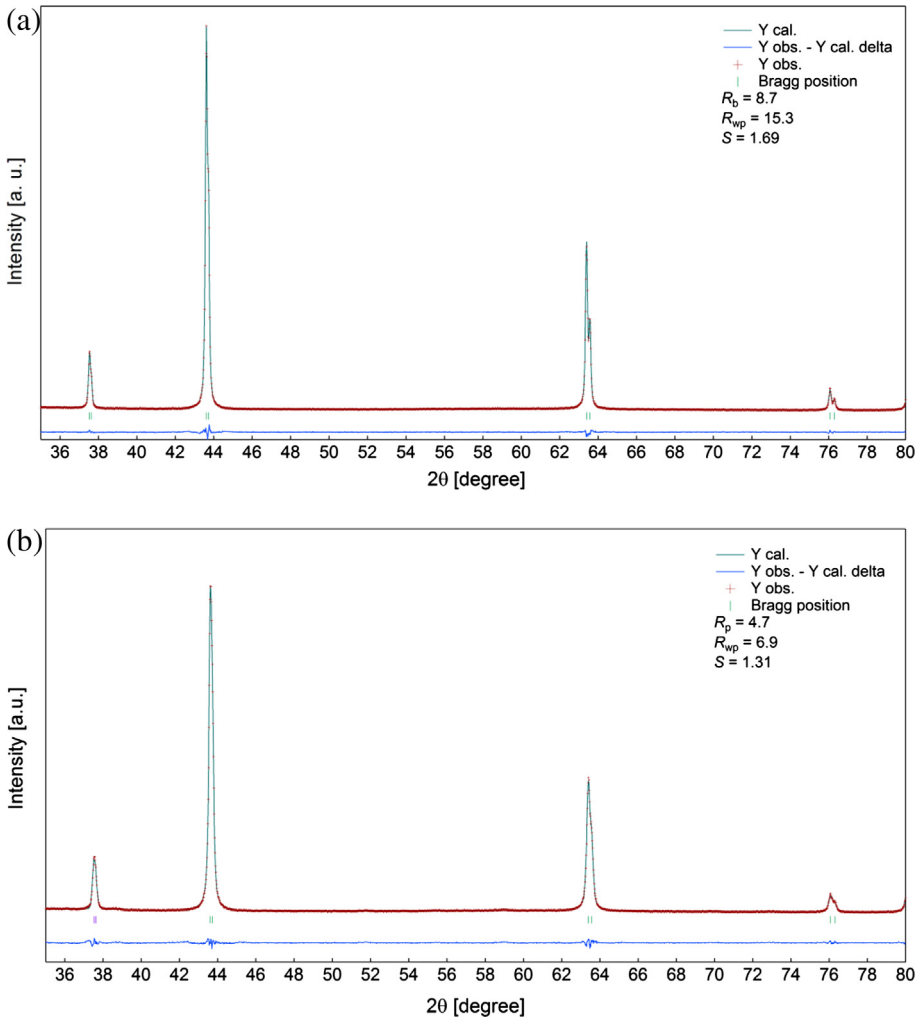

Fig. 3. Observed (dot) and calculated (solid line) X-ray diffraction profiles of (a) Li_2NiTiO_4 and (b) $Li_2NiSi_{0.1}Ti_{0.9}O_4$. The difference between the observed and calculated profiles is plotted below.

has a rigid framework without Van der Waals gap, because all oxygen is shared with four MO_6 cluster, as shown Fig. 1(a). The lithium ion for rocksalt Li_2NiTiO_4 in charge process migrates from pristine 4*b* octahedral to tetrahedral 8*c* sites [11]. In addition, the oxygen atoms located out of sequence in the disorder matrix could easily escape during the charging process [12, 13]. Therefore, it has a large irreversible capacity of over 80 mAh g^{-1} at the first cycle [12]. In order to reduce the large irreversible capacity, we tried to decrease the crystallinity and the particle size of Li_2NiTiO_4 by substituting smaller Si^{4+} (0.400 Å) for Ti^{4+} (0.605 Å). As far as we know, the previous report about the end member Li_2NiSiO_4 as shown Fig. 1(b) is only one. It described the Li intercalated potential computed with the GGA+U method [14]. We are interested in the electrochemical properties of Li_2NiTiO_4, which has same composition as Li_2NiSiO_4, by substituting Si^{4+} for Ti^{4+}. Moreover, we also expected that the theoretical capacity of Li_2NiTiO_4 increases with the substituting of titanium by lighter weight Si (28.08 g mol^{-1}) than Ti (47.88 g mol^{-1}). To improve the cathode properties, the amount of Si doping to Li_2NiTiO_4 was optimized, and the doped cathode performances were evaluated. In addition, the crystal structure changes during the charge and discharge reaction were measured by X-ray diffraction method.

2. Experiment

Li_2NiTiO_4 and $Li_2NiSi_xTi_{1-x}O_4$ were synthesized using the methods previously described [12]. Stoichiometric ratios of $LiNO_3$, $Ni(NO_3)_2 \cdot 6H_2O$, titanium(IV) butoxide and tetraethylorthosilicate (TEOS) required to produce Si-doped Li_2NiTiO_4 were dissolved in water. Here, $Li_2NiSi_{0.1}Ti_{0.9}O_4$ was prepared by using TEOS or SiO_2 nano-powder as a Si source. To the above solution, the required quantity of citric acid crystals was added and mixed thoroughly for 30 min at 70 °C in a heating mantle; then the temperature was increased to 110 °C to evaporate the solvents and water. Evaporation was continued in the mantle itself to obtain a dry mass. The precursor was sintered at 300 °C for 3 h with an electric oven. After cooling in the oven, the sintered mixture was mixed and ground, then sintered again at 600 °C for 14 h. Hereinafter, the obtained $Li_2NiSi_{0.1}Ti_{0.9}O_4$ samples prepared with TEOS and SiO_2 nano-powder are referred to as $Li_2NiTi_{0.9}Si_{0.1}O_4$ (TEOS as a Si source) and $Li_2NiTi_{0.9}Si_{0.1}O_4$ (SiO_2 as a Si source), respectively, and $Li_2NiTi_{0.9}Si_{0.1}O_4$ refers to the both samples except as otherwise noted.

The 70 wt. % powder that was obtained was dry-ball-milled with 25 wt. % acetylene black (Denki Kagaku Co., Ltd.). Cathodes for electrochemical performance were prepared by mixing the $Li_2NiSi_xTi_{1-x}O_4$/C composite powder with a 5 wt. % PVDF binder (KurehaCorp.) in *N*-methylpyrrolidione. The slurry was coated on aluminum foil and dried at 80 °C until the solvent had evaporated completely. Cathode pellets for structure change during the charge–discharge cycle were fabricated by mixing the $Li_2NiSi_xTi_{1-x}O_4$/C composite powder with 5% polytetrafluoroethylene (PTFE) Teflon binder (Polyflon PTFE F-103, Daikin Industry, Ltd.) and punched in the form of disks (ca. 30 mg weight and 10 mm diameter). The electrochemical performance of the obtained products was evaluated with a 2032 coin-type cell using a non-aqueous electrolyte (1 M $LiPF_6$/EC:DMC = 1:1 in volume, Kishida Chemical Co., Ltd.) and a polypropylene separator (Celgard 3501) against lithium metal (Honjo Metal Co., Ltd.). All the cells were assembled in an Ar-filled glove box. The charge–discharge measurement was performed in galvanostatic mode at a rate of 16 mA g^{-1}. The test temperature was 25 °C. The electrodes were carefully taken out from the cells in the Ar-filled glove box, washed, and immersed with DMC for one night to remove the electrolyte, and dried prior to being set in an Ar-filled cell for XRD.

The XRD data for the pellet samples was taken under Ar because of the instability of the transition metal valence in air. Characterization of the obtained powder and pellets after the charge or discharge processes was carried out with an X-ray powder diffractometer (XRD, 50 kV and 300 mA, CuKα, Rigaku Corp., TTRIII).

Surface observation and chemical species mapping of obtained products were performed with a TOF-SIMS apparatus [15]. This apparatus features single-particle analysis with high lateral resolution (down to 40 nm) [15]. The apparatus has two beams: a focused ion beam (FIB) and an electron beam (EB). The FIB was used to section a particle, observe the surface, and obtain the chemical mapping. The EB was used for the observation during the FIB sectioning. A 30-keV Ga+ focused ion beam was rastered over a sample area of 10 μm × 10 μm to obtain the SIM image. The Ga^+ ion current was approximately 150 pA. Pulsed Ga^+ was used as the primary ion beam for elemental mapping.

The composition of $Li_2NiSi_xTi_{1-x}O_4$ (x = 0, 0.1) powder and pellets was determined by means of an Atomic Absorption Spectrometry (AAS, Z-2300, Hitachi Ltd.) following the pretreatment with the conc.

3. Results and discussion

3.1. Characterization of obtained $Li_2NiSi_xTi_{1-x}O_4$

The crystal structure of the obtained $Li_2NiSi_xTi_{1-x}O_4$ ($x = 0 \sim 0.5$) was characterized with XRD, as shown in Fig. 2. $Li_2NiSi_xTi_{1-x}O_4$ ($x = 0, 0.1, 0.2$) obtained from the liquid phase could be indexed as a cubic system with the space group *Fm*-3*m* as we expected.

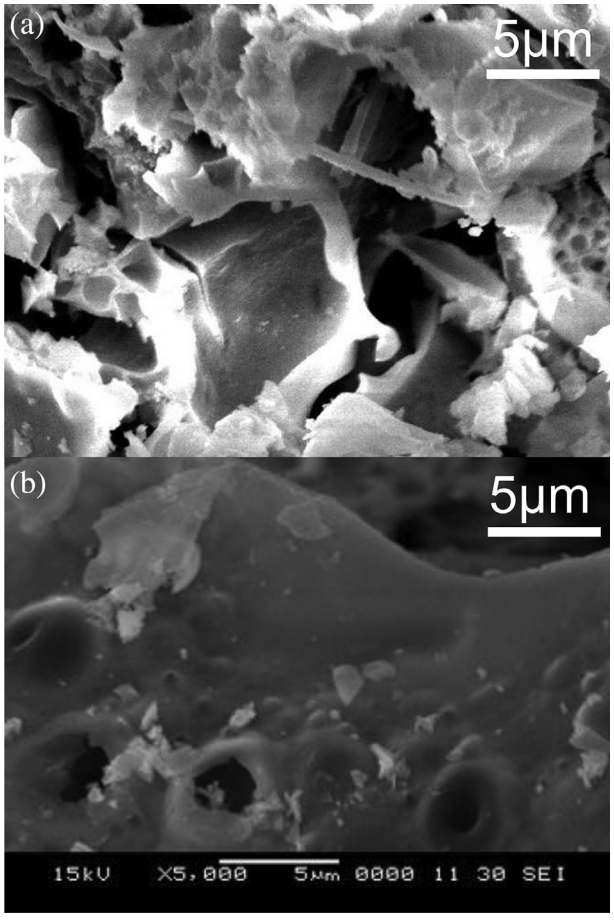

Fig. 4. SEM images of the obtained (a) Li_2NiTiO_4 and (b) $Li_2NiSi_{0.1}Ti_{0.9}O_4$.

However, it was difficult to obtain single-phase for $Li_2NiSi_xTi_{1-x}O_4$ ($x \geq 0.3$), and a small amount of SiO_2 and/or Li_2SiO_3 were included as the impurities. The calculated and experimental diffraction pattern for Li_2NiTiO_4 is shown in Fig. 3(a) [16]. The peaks are quite sharp, indicating the good crystallinity of the material. The lattice constant of $a = 4.1406$ (7) Å and the cell volume $V = 70.9924$ Å^3 obtained from the refined Li_2NiTiO_4 were in good agreement with previously reported values [12]. The lattice constant obtained from the refined $Li_2NiSi_{0.1}Ti_{0.9}O_4$ was $a = 4.1394(0)$ and the cell volume $V = 70.9270$ Å^3 (Fig. 3(b)). These lattice constant of $Li_2NiSi_xTi_{1-x}O_4$ did not change, while the XRD peak width expanded as the Si doping level increased. It suggests that the crystallinity was reduced with only a small amount of Si doping. The structure of cubic rocksalt-type $Li_2NiSi_xTi_{1-x}O_4$ consists of Li^+ (0.76 Å), Ni^{2+} (0.69 Å) and Ti^{4+} (0.605 Å) ions residing in 4*b* sites, and O^{2-} ions distributed in the 4*a* sites. Therefore, it is considered that the doped Si^{4+} (0.400 Å) occupied the 4*b* site. Although the relatively smaller $Si^{4+}$was substituted for the Ti^{4+}, the cell volume and the crystal structure of $Li_2NiSi_xTi_{1-x}O_4$ was maintained due to the larger ion radii of Li, Ni and Ti than that of Si. However, Si^{4+} is usually in the tetrahedral site, not in the octahedral site. Therefore, the formation of SiO_2 in the grain boundary might reduce the particle size and contribute the better cathode performances, because the lattice constant of $Li_2NiSi_xTi_{1-x}O_4$ did not change by Si doping level increased. We observed the particle surfaces of Li_2NiTiO_4 and $Li_2NiTi_{0.9}Si_{0.1}O_4$ (TEOS as a Si source) by SEM (Fig. 4), and compared the dispersion state of Si for the particle surfaces and the cross section in $Li_2NiTi_{0.9}Si_{0.1}O_4$ (TEOS as a Si source) and $Li_2NiTi_{0.9}Si_{0.1}O_4$ (SiO_2 as a Si source) by TOF-SIMES (Fig. 5). Si on the particle surfaces was hardly observed in $Li_2NiTi_{0.9}Si_{0.1}O_4$ (TEOS as a Si source,

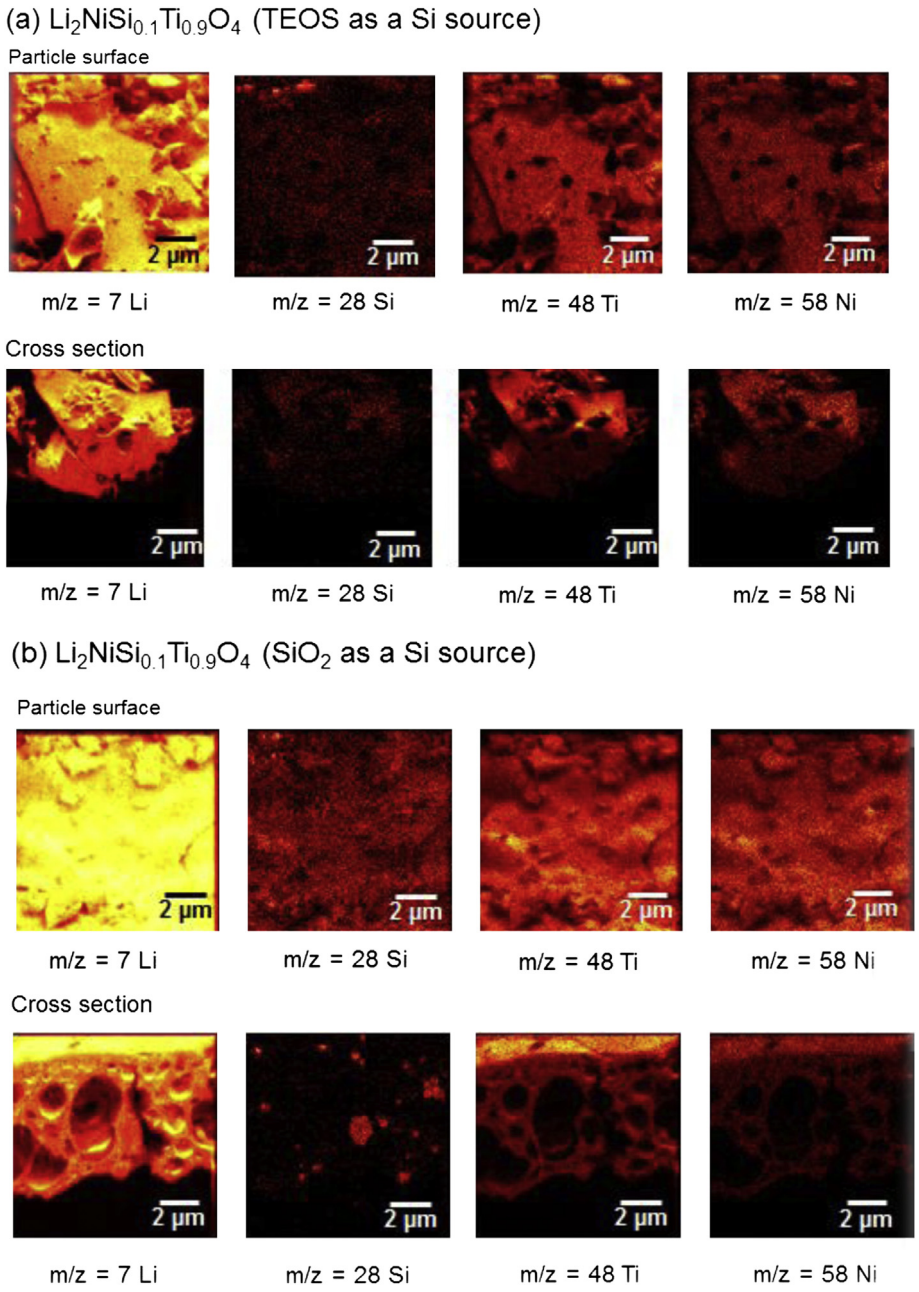

Fig. 5. TOF-SIMS elemental maps for the obtained (a) $Li_2NiSi_{0.1}Ti_{0.9}O_4$ (TEOS as a Si source) and (b) $Li_2NiSi_{0.1}Ti_{0.9}O_4$ (SiO_2 as a Si source).

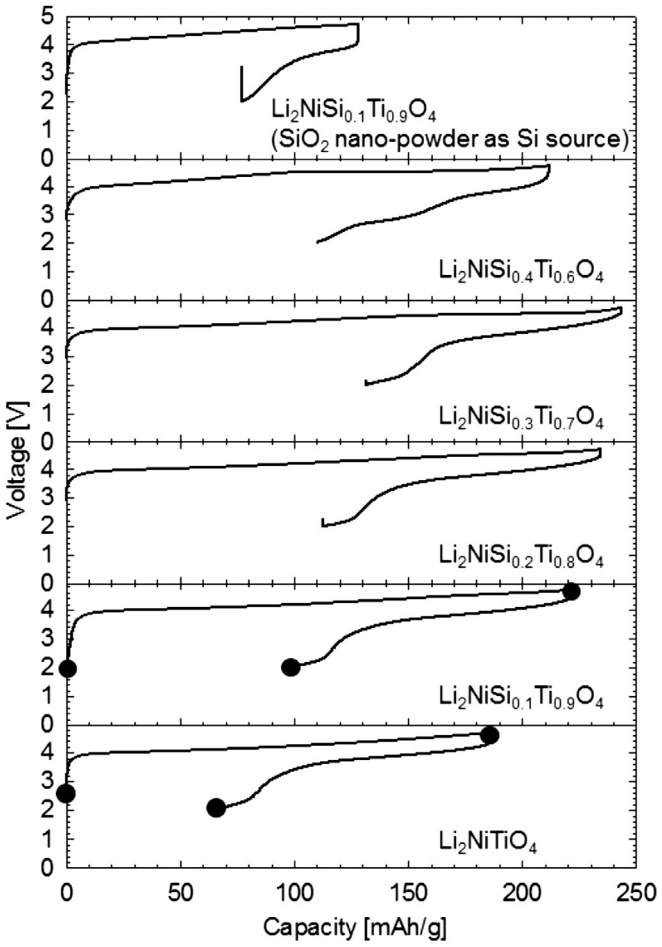

Fig. 6. Initial charge and discharge curves for $Li_2NiSi_xTi_{1-x}O_4$ ($x = 0 \sim 0.5$) and $Li_2NiSi_{0.1}Ti_{0.9}O_4$ (SiO_2 as a Si source) against an Li anode at a rate of 16 mA g^{-1}. Electrochemical measurements were carried out with a potential window between 2.0 and 4.7 V. The symbols (●) represent the sampling points for the *ex-situ* XRD measurement (Figs. 8 and 9).

Fig. 5(a)) and $Li_2NiTi_{0.9}Si_{0.1}O_4$ (SiO_2 as a Si source, Fig. 5(b)). On the other hand, the ununiform deposit of Si particles were observed in the cross section of $Li_2NiTi_{0.9}Si_{0.1}O_4$ (SiO_2 as a Si source), while Si seems to be dispersed uniformly in the cross section of $Li_2NiTi_{0.9}Si_{0.1}O_4$ (TEOS as a Si source). It suggested that most of dopant Si in $Li_2NiTi_{0.9}Si_{0.1}O_4$ (TEOS as a Si source) was substituted for Ti. Moreover, the crystallinity of $Li_2NiTi_{0.9}Si_{0.1}O_4$ was lower than that of Li_2NiTiO_4. It also suggests that the crystal growth of $Li_2NiTi_{0.9}Si_{0.1}O_4$ was inhibited by Si doping.

3.2. Cathode properties for obtained $Li_2NiSi_xTi_{1-x}O_4$ vs. Li cell

Fig. 6 shows the initial charge (Li^+ extraction) and discharge (Li^+ insertion) curves of the obtained $Li_2NiSi_xTi_{1-x}O_4$ at rate of 16 mA g^{-1}. The electrochemical measurements were carried out with a potential window between 2.0 and 4.7 V. The initial charge and discharge capacities of Li_2NiTiO_4 were 186 mAh g^{-1} and 120 mAh g^{-1} with a 65% discharge/charge efficiency. The charge

Table 1
The initial charge and discharge capacity of $Li_2NiSi_{0.1}Ti_{0.9}O_4$ ($0 \le x \le 0.4$) at rate of 16 mA g^{-1}.

Si doping level	$x = 0$	$x = 0.1$	$x = 0.2$	$x = 0.3$	$x = 0.4$
Initial charge capacity [mAh g^{-1}]	186.1	221.1	234.3	252.3	230.0
First discharge capacity [mAh g^{-1}]	120.4	123.3	121.4	112.6	113.8

Table 2
Correlation between the amount of electron transfer and the detected Li content by AAS measurement.

Sample state	$LiNiTiO_4$		$Li_2NiSi_{0.1}Ti_{0.9}O_4$	
	Amount of electron transfer [e^-]/[$NiTiO_4$]	Detected Li content by AAS measurement [Li]/[$NiTiO_4$]	Amount of electron transfer [e^-]/[$NiTiO_4$]	Detected Li content by AAS measurement [Li]/[$NiTiO_4$]
Initial state	–	–	–	–
After charge until 4.7 V	1.28	1.06	1.51	1.50
After discharge until 2.0 V	0.82	0.77	0.85	0.77

capacity of $Li_2NiSi_xTi_{1-x}O_4$ increased compared with Li_2NiTiO_4 until $x = 0.3$ in $Li_2NiSi_xTi_{1-x}O_4$, and the discharge capacity was largest at $x = 0.1$ in $Li_2NiSi_xTi_{1-x}O_4$, as shown in Table 1. On the other hand, the charge and discharge capacity of $Li_2NiSi_{0.1}Ti_{0.9}O_4$ (SiO_2 as a Si source) was 128 mAh g^{-1} and 51 mAh g^{-1}, respectively. The poor cathode performances must have been caused by the ununiform deposit of SiO_2 particle in $Li_2NiSi_{0.1}Ti_{0.9}O_4$ (SiO_2 as a Si source) as shown in Fig. 5(b). Moreover, Li_2NiTiO_4 and $Li_2NiSi_xTi_{1-x}O_4$ had two discharge plateaus of 3.9 V and 2.0 V. According to the result, we supposed that the charge–discharge reaction around 3.9 V was generated by Ni^{2+}/Ni^{3+} redox and that around 2.0 V was by Ti^{3+}/Ti^{4+}. In addition, the results of the AAS measurement suggest that this charge–discharge reaction has occurred with extraction/insertion of lithium, and that the charge reaction does not include other side reactions such as electrolyte decomposition, as shown in Table 2. Fig. 7 shows the cyclability of the obtained Li_2NiTiO_4 and $Li_2NiSi_{0.1}Ti_{0.9}TiO_4$. The discharge capacities of Li_2NiTiO_4 and $Li_2NiSi_{0.1}Ti_{0.9}TiO_4$ remained at 57 mAh g^{-1} and 76 mAh g^{-1} even after 20 cycles, respectively. In addition, the cubic rocksalt-type cathode materials had a large irreversible capacity at the first cycle of ca. 60 mAh g^{-1}. To solve this problem, electrochemical measurements of Li_2NiTiO_4 and $Li_2NiSi_{0.1}Ti_{0.9}O_4$ were carried out at rate of 7.8 mA g^{-1} (charge process) and 0.38 mA g^{-1} (discharge process). The initial charge and discharge capacities of Li_2NiTiO_4 were 174 mAh g^{-1} and 153 mAh g^{-1} with a 88% discharge/charge efficiency (Fig. 8). On the other hand, the initial charge and discharge

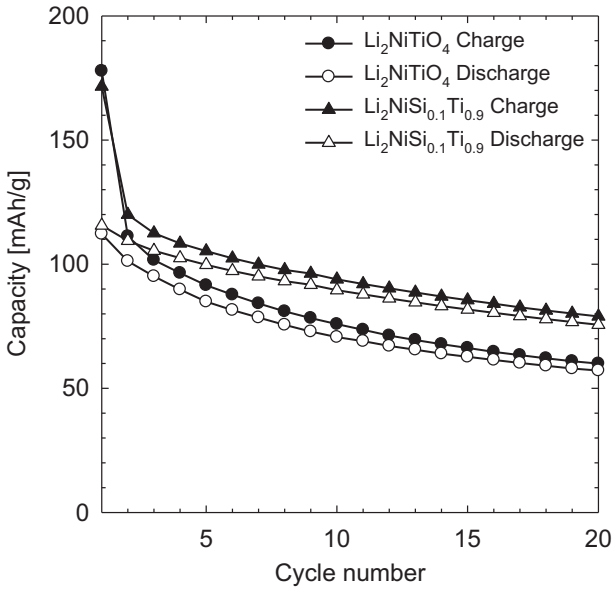

Fig. 7. Cyclabilities for Li_2NiTiO_4 and $Li_2NiSi_{0.1}Ti_{0.9}O_4$ against an Li anode in the potential window between 2.0 and 4.7 V at the rate of 16 mA g^{-1}.

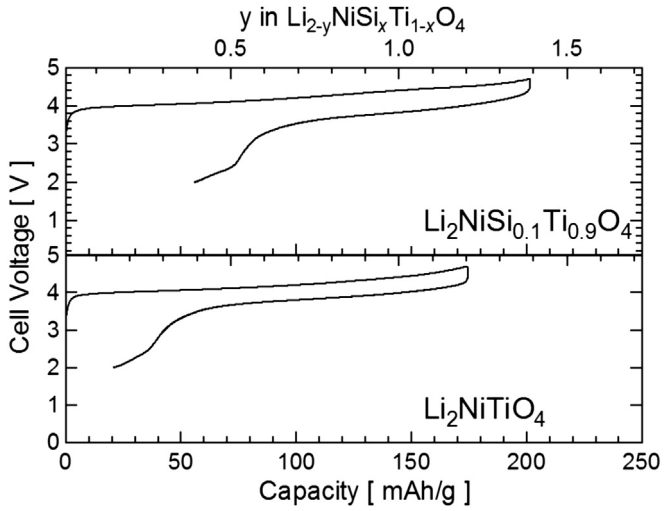

Fig. 8. The initial charge and discharge curves for Li_2NiTiO_4 and $Li_2NiSi_{0.1}Ti_{0.9}O_4$ against an Li anode at the rate of 16 mA g^{-1} (charge) and 0.32 mA g^{-1} (discharge).

capacities of $Li_2NiSi_{0.1}Ti_{0.9}O_4$ were 202 mAh g^{-1} and 146 mAh g^{-1} with a 72% discharge/charge efficiency. The irreversible capacity of Li_2NiTiO_4 and $Li_2NiSi_{0.1}Ti_{0.9}O_4$ was improved by inserting Li^+ into the $Li_{2-y}NiTiO_4$ or $Li_{2-y}NiSi_{0.1}Ti_{0.9}O_4$ ($0 < y < 2$) structure at a low rate. The energy densities at the rate of 0.32 mA g^{-1} of the obtained Li_2NiTiO_4 and $Li_2NiSi_{0.1}Ti_{0.9}O_4$ were equivalent to that of $LiCoO_2$.

3.3. Structural changes to $LiNiTiO_4$ and $Li_2NiSi_{0.1}Ti_{0.9}O_4$ during the first charge and discharge process

We investigated the structural change of $LiNiTiO_4$ and $Li_2NiSi_{0.1}Ti_{0.9}O_4$ for the initial charge and discharge cycle by *ex-situ* XRD measurements. The XRD measurements were performed on three samples of $LiNiTiO_4$ and $Li_2NiSi_{0.1}Ti_{0.9}O_4$ pellets during the charge and discharge cycle, as shown in Fig. 6, under an Ar atmosphere. Fig. 9 compares the XRD profiles of electrode pellets of $LiNiTiO_4$ at (a) the initial state, (b) the charge endpoint, and (c) the discharge

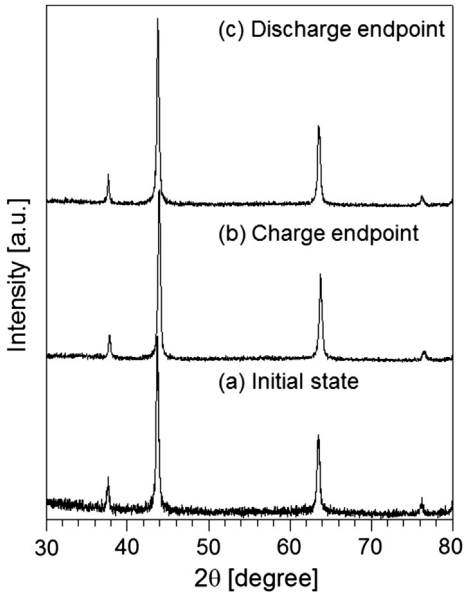

Fig. 9. *Ex-situ* XRD profiles of a Li_2NiTiO_4 against an Li anode during the initial charge–discharge cycle; (a) initial Li_2NiTiO_4 state, and (b) electrode pellet for the charge endpoint and (c) discharge endpoint, respectively.

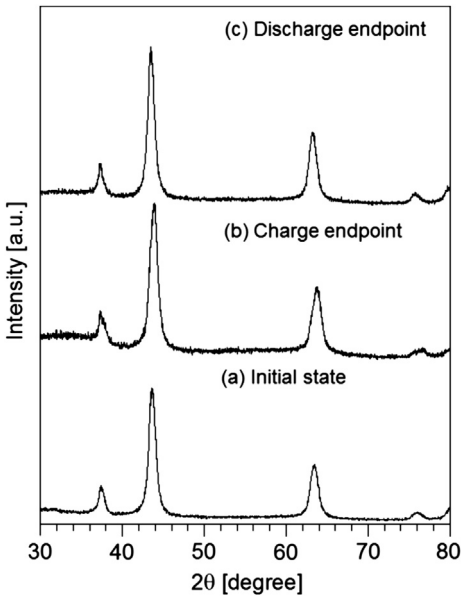

Fig. 10. *Ex-situ* XRD profiles of $Li_2NiSi_{0.1}Ti_{0.9}O_4$ against an Li anode during the initial charge–discharge cycle; (a) initial $Li_2NiSi_{0.1}Ti_{0.9}O_4$ state, and (b) electrode pellet for the charge endpoint and (c) discharge endpoint, respectively.

endpoint. All XRD diffraction peaks shifted to a higher 2θ angle from that of the initial state on the initial charge process, and moved back to almost the original position after the first discharge process. The change of the a axis of Li_2NiTiO_4 during the first charge–discharge process was 4.14 Å (initial state) → 4.12 Å (charge endpoint) → 4.14 Å (discharge endpoint). Meanwhile, the unit cell volumes were 71.0 $Å^3$ (initial state), 69.9 $Å^3$ (charge endpoint), and 71.0 $Å^3$ (discharge endpoint), respectively. Fig. 10 shows the XRD profiles of electrode pellets of $Li_2NiSi_{0.1}Ti_{0.9}O_4$ at (a) the initial state, (b) the charge endpoint and (c) the discharge endpoint. All XRD diffraction peaks of $Li_2NiSi_{0.1}Ti_{0.9}O_4$ moved to a higher 2θ angle, and moved back to almost the original position during the first charge–discharge process. No generation of impurities was found on XRD profiles during the charge–discharge process. The lattice constant of the initial state of $Li_2NiSi_{0.1}Ti_{0.9}O_4$ was $a = 4.15$ Å and the unit cell volume was 71.5 $Å^3$, while $a = 4.13$ Å and the unit cell volume was 70.4 $Å^3$ at the charge endpoint. In particular, the unit cell volume change of $Li_2NiSi_{0.1}Ti_{0.9}O_4$ accompanying the extraction/insertion of lithium was only −1.5%, which was same as that of Li_2NiTiO_4 (−1.5%), although the many Li in charge process was extracted from $Li_2NiSi_{0.1}Ti_{0.9}O_4$ than that from Li_2NiTiO_4 as shown in Table 2. The unit cell volume change for cubic rocksalt-type materials accompanying the extraction/insertion of lithium was hardly changed even if Ti in Li_2NiTiO_4 was substituted to Si with a smaller ionic radius. These results suggest that the framework of Li_2NiTiO_4 and $Li_2NiSi_xTi_{1-x}O_4$ is stable enough to maintain the charge–discharge processes at the first cycle by the expansion and contraction of the lattice accompanying the extraction/insertion of lithium.

4. Conclusion

$Li_2NiSi_xTi_{1-x}O_4$ cathode materials were obtained by a sol–gel method under ambient pressure in the whole $0 \le x \le 0.2$ regions. The crystallinity of the obtained $Li_2NiSi_xTi_{1-x}O_4$ was less than that of Li_2NiTiO_4. At a low rate condition (0.32 mA g^{-1}), the first discharge capacity of Li_2NiTiO_4 and $Li_2NiSi_{0.1}Ti_{0.9}O_4$ were 153 mAh g^{-1} and 146 mAh g^{-1}, respectively. However, the initial rechargeable capacities were improved by Si doping at a relatively

high rate condition. XRD measurement proved that the volume change ratio during cycling is only 1.5%. Although rigid framework without van der Waals gap such as cubic rocksalt Li_2NiTiO_4 is not actually suitable for high rate Li kinetics, it seems to be an advantageous structure, in the case of low rate cycle such as load leveling.

Acknowledgments

The authors are grateful to Ms. Mariko Komoto, Mr. Yoshihiro Yamamoto and Mr. Tokuo Inamasu of GS Yuasa Corporation for their experimental assistance. TOF-SIMS measurements were conducted with help of Dr. Takeharu Ishikawa of Toyama Co., Ltd.

References

[1] W. Li, J.C. Currie, J. Wolstenholme, J. Power Sources 68 (1997) 565.
[2] G. Dutta, A. Manthiram, J.B. Goodenough, J. Solid State Chem. 96 (1992) 123.
[3] A. Hirano, R. Kanno, Y. Kawamoto, Y. Takeda, K. Yamamura, M. Takano, K. Ohyama, M. Ohashi, Y. Yamaguchi, Solid State Ionics 78 (1995) 123.
[4] Y. Makimura, T. Ohzuku, J. Power Sources 119–121 (2003) 156.
[5] W.S. Yoon, C.P. Grey, M. Balasubramanian, X.Q. Yang, J. McBreen, Chem. Mater. 15 (2003) 3161.
[6] T.A. Sasaki, T. Soga, Physica 111B (1981) 304.
[7] M. Tsuda, H. Arai, M. Takahashi, H. Ohtsuka, Y. Sakurai, K. Sumitomo, H. Kageshima, J. Power Sources 144 (2005) 183.
[8] L. Sebastian, J. Gopalakrishnan, J. Solid State Chem. 172 (2003) 171.
[9] M. Yang, X. Zhao, Y. Bian, L. Ma, L. Ma, Y. Ding, X. Shen, J. Mater. Chem. 22 (2012) 6200.
[10] M. Kuzma, R. Dominko, A. Medan, D. Makovec, M. Bele, J. Jamnlk, M. Gaberscek, J. Power Sources 189 (2009) 81.
[11] R. Trocoli, M. Crus-Yusta, J. Morales, J. Santos-Pena, Electrochim. Acta 100 (2013) 93.
[12] S.R.S. Prabaharan, M.S. Michael, H. Ikuta, Y. Uchimoto, M. Wakihara, Solid State Ionics 172 (2004) 39.
[13] Z. Lu, J.R. Dahn, J. Electrochem. Soc. 149 (2002) A815.
[14] M.E. Arroyo-de Dompablo, M. Armand, J.M. Tarascon, U. Amador, Electrochem. Commun. 8 (2006) 1292.
[15] T. Sakamoto, M. Koizumi, J. Kawasaki, J. Yamaguchi, Appl. Surf. Sci. 225 (2008) 1617.
[16] F. Izumi, K. Momma, Solid State Phenom. 130 (2007) 15.